

Mid-infrared near-field spectroscopy

Sergiu Amarie*, Thomas Ganz, and Fritz Keilmann

Max Planck Institute for Quantum Optics, 85741 Garching, Germany

*samarie@rzg.mpg.de

Abstract: We demonstrate *continuous* infrared spectra from 20 nm sample spots, by combining dispersive Fourier-transform infrared spectroscopy (FTIR) with scattering near-field microscopy (s-SNOM). With the “apertureless” tip of a standard AFM cantilever in one arm of a Michelson interferometer the spectra arise simultaneously in amplitude and phase. The effect of near-field phonon resonance of SiC is used to verify background-free s-SNOM operation, and to determine the absolute scattering efficiency, at 6 cm^{-1} spectral resolution. We further report first evidence of free-induction decay from a scatterer composed of parts coupled by near-fields. This is possible only with broadband illumination. It offers a new, unique tool to discriminate against background scattering artifacts.

©2009 Optical Society of America

OCIS codes: (160.2710) Inhomogeneous optical media; (180.4243) Near-field microscopy; (300.6340) Spectroscopy, infrared; (300.6300) Spectroscopy, Fourier transforms.

References and links

1. F. Keilmann, and R. Hillenbrand, “Near-field nanoscopy by elastic light scattering from a tip,” in *Nano-Optics and Near-Field Optical Microscopy*, A. Zayats and D. Richards, eds. (Artech House, 2009).
2. M. M. Qazilbash, M. Brehm, B. G. Chae, P. C. Ho, G. O. Andreev, B. J. Kim, S. J. Yun, A. V. Balatsky, M. B. Maple, F. Keilmann, H. T. Kim, and D. N. Basov, “Mott transition in VO₂ revealed by infrared spectroscopy and nano-imaging,” *Science* **318**(5857), 1750–1753 (2007).
3. A. J. Huber, D. Kazantsev, F. Keilmann, J. Wittborn, and R. Hillenbrand, “Simultaneous infrared material recognition and conductivity mapping by nanoscale near-field microscopy,” *Adv. Mater.* **19**(17), 2209–2212 (2007).
4. R. Hillenbrand, T. Taubner, and F. Keilmann, “Phonon-enhanced light matter interaction at the nanometre scale,” *Nature* **418**(6894), 159–162 (2002).
5. T. Taubner, R. Hillenbrand, and F. Keilmann, “Nanoscale polymer recognition by spectral signature in scattering infrared near-field microscopy,” *Appl. Phys. Lett.* **85**(21), 5064–5066 (2004).
6. M. Brehm, T. Taubner, R. Hillenbrand, and F. Keilmann, “Infrared spectroscopic mapping of single nanoparticles and viruses at nanoscale resolution,” *Nano Lett.* **6**(7), 1307–1310 (2006).
7. I. Kopf, J. S. Samson, G. Wollny, C. Grunwald, E. Bründermann, and M. Havenith, “Chemical imaging of microstructured self-assembled monolayers with nanometer resolution,” *J. Phys. Chem. C* **111**(23), 8166–8171 (2007).
8. K. Mueller, X. Yang, M. Paulite, Z. Fakhraai, N. Gunari, and G. C. Walker, “Chemical imaging of the surface of self-assembled polystyrene-b-poly(methyl methacrylate) diblock copolymer films using apertureless near-field IR microscopy,” *Langmuir* **24**(13), 6946–6951 (2008).
9. M. Brehm, A. Schliesser, and F. Keilmann, “Spectroscopic near-field microscopy using frequency combs in the mid-infrared,” *Opt. Express* **14**(23), 11222–11233 (2006).
10. N. Ocelic, A. Huber, and R. Hillenbrand, “Pseudo-heterodyne detection for background-free near-field spectroscopy,” *App. Phys. Lett.* **89**, 101124–101121 - 101124–101123 (2006).
11. B. Knoll, and F. Keilmann, “Enhanced dielectric contrast in scattering-type scanning near-field optical microscopy,” *Opt. Commun.* **182**(4-6), 321–328 (2000).
12. H. G. von Ribbeck, M. Brehm, D. W. van der Weide, S. Winnerl, O. Drachenko, M. Helm, and F. Keilmann, “Spectroscopic THz near-field microscope,” *Opt. Express* **16**(5), 3430–3438 (2008).
13. M. Brehm, A. Schliesser, F. Cajko, I. Tsukerman, and F. Keilmann, “Antenna-mediated back-scattering efficiency in infrared near-field microscopy,” *Opt. Express* **16**(15), 11203–11215 (2008).
14. T. Taubner, F. Keilmann, and R. Hillenbrand, “Nanomechanical resonance tuning and phase effects in optical near-field interaction,” *Nano Lett.* **4**(9), 1669–1672 (2004).
15. A. Huber, N. Ocelic, T. Taubner, and R. Hillenbrand, “Nanoscale resolved infrared probing of crystal structure and of plasmon-phonon coupling,” *Nano Lett.* **6**(4), 774–778 (2006).
16. A. J. Huber, A. Ziegler, T. Köck, and R. Hillenbrand, “Infrared nanoscopy of strained semiconductors,” *Nat. Nanotechnol.* **4**(3), 153–157 (2009).
17. A. Cvitkovic, N. Ocelic, and R. Hillenbrand, “Analytical model for quantitative prediction of material contrasts in scattering-type near-field optical microscopy,” *Opt. Express* **15**(14), 8550–8565 (2007).

18. F. Keilmann, "Surface-polariton propagation for scanning near-field optical microscopy application," *J. Microsc.* **194**(2-3), 567–570 (1999).
19. M. Stockman, "Nanofocusing of optical energy in tapered plasmonic waveguides," *Phys. Rev. Lett.* **93**, 137404 (2004).
20. P. G. Gucciardi, G. Bachelier, M. Allegrini, J. Ahn, M. Hong, S. H. Chang, W. Ihe, S. C. Hong, and S. H. Baek, "Artifacts identification in apertureless near-field optical microscopy," *J. Appl. Phys.* **101**, 64303–64308 (2007).
21. N. Ocelic, "Quantitative near-field phonon-polariton spectroscopy," *Thesis Technische Universität München*, ISBN 9783932749896 (2007).
22. R. Hillenbrand, and F. Keilmann, "Optical oscillation modes of plasmon particles observed in direct space by phase-contrast near-field microscopy," *Appl. Phys. B* **73**, 239–243 (2001).
23. R. Hillenbrand, F. Keilmann, P. Hanarp, D. S. Sutherland, and J. Aizpurua, "Coherent imaging of nanoscale plasmon patterns with a carbon nanotube optical probe," *Appl. Phys. Lett.* **83**(2), 368–370 (2003).
24. M. Schnell, A. Garcia-Etxarri, A. J. Huber, K. Crozier, J. Aizpurua, and R. Hillenbrand, "Controlling the near-field oscillations of loaded plasmonic nanoantennas," *Nat. Photonics* **3**(5), 287–291 (2009).
25. A. Huber, N. Ocelic, D. Kazentsev, and R. Hillenbrand, "Near-field imaging of mid-infrared surface phonon polariton propagation," *Appl. Phys. Lett.* **87**, 81103 (2005).

1. Introduction

Near-field microscopy by Rayleigh scattering from a tip has the proven potential of tip-limited resolution of typically 20 nm. This is independent of the wavelength which can be chosen throughout the visible, infrared, THz and even microwave regions [1]. Disturbing "background" scattering from parts outside the tip's apex region are routinely suppressed by tapping the tip against the sample and demodulating the light signal at the tapping frequency or its harmonics. Numerous applications have been established using *monochromatic s-SNOM*, for example, the detection of nanosize metallic regions that occur in the insulator-metal phase transition [2], or the quantitative mapping of free-carrier concentration in semiconductor nanodevices [3]. Yet the future impact of s-SNOM requires a *spectroscopic* operation exploiting the infrared and far-infrared vibrational fingerprints. These are routinely assessed in research and industry, using FTIR spectrometers for identification and quantifying chemical composition. Monochromatic s-SNOM has already succeeded in mapping vibrational resonances by repeated s-SNOM imaging at varied frequency, and subsequent extraction of spectra [4–8]. This procedure is, however, rather laborious and prone to errors from non-reproducibilities of the scan process. For example, the sample might drift, the tapping conditions might change, and the tip might erode or pick up debris.

2. Design of broadband s-SNOM

Our present experiment uses spectrally broadband illumination of a novel, commercial s-SNOM (NeaSNOM, neaspec.com), for recording a spectrum at each pixel while scanning (Fig. 1).

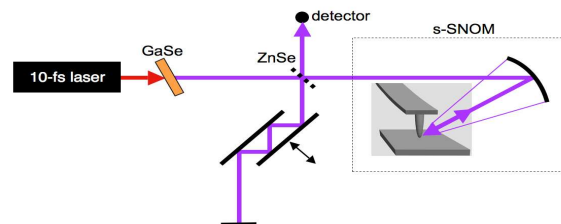


Fig. 1. Sketch of spectroscopic near-field microscope where the back-scattering probe tip represents one end mirror of a dispersive Michelson interferometer. A mirror in the reference arm is mechanically translated to record an interferogram which is then Fourier-transformed to determine both amplitude and phase spectra.

Interferometric operation is achieved by a dispersive Michelson configuration, resembling the earlier homodyne [5], multi-heterodyne [9], and pseudo-heterodyne setups [10]. The reference arm's length is continuously varied and an interferogram is recorded for subsequent Fourier-transformation (FT). We use a coherent beam with a broad spectrum resulting from difference-frequency generation in a 200 μm thick GaSe crystal (ATOM, eletot.tsu.ru), of 10-

fs Ti:S laser pulses at 125 MHz repetition and 500 mW quasi-c.w. power. The crystal is oriented to generate the band between 9 and 12 μm at 5 μW quasi-c.w. power. The back-scattered infrared beam is partially reflected at the beam splitter, a 2 mm thick uncoated ZnSe plate, and focused on a HgCdTe detector (KLD-0.25-J1, kolmar.com). The signal is amplified by 60 db (HVA-10M-60-B, femto.de) and processed in a lock-in amplifier (EG&G5302, princetonappliedresearch.com). The s-SNOM's focusing mirror has about 20 mm effective focal length and accepts a collimated beam in a 15 mm aperture. The incident beam is at about 30° inclination to the horizontal sample surface and is vertically polarized. The sample is scanned while the commercial cantilevered Pt-coated tip (PPP-NCHPt-20, nanosensors.com) is fixed and oscillates at 310 kHz. An integrated microscope provides a top view of the sample, the cantilever, the AFM laser spot, and the illuminating spot which helps in the alignment of both the AFM and s-SNOM operations.

The recording of interferograms is done with an oscilloscope (Wavesurfer 422, lecroyc.com). This also performs on-line FT for previewing spectra at 20 cm^{-1} resolution, as limited by nonlinearity in the mirror translation stage (P-628, pi.ws). We overcome this constraint by off-line resampling according to frequent calibration interferograms taken with a CO_2 laser beam, set at about $100\text{ }\mu\text{W}$ by a step attenuator (102, lasnix.com). With our choice of 1.7 mm long interferograms taken in 2 s the resolution becomes 6 cm^{-1} . The interferometer arm length of about 25 cm is found sufficiently short to keep, in the thermostatted laboratory, thermal drifts small enough that the phase calibration stays valid over hours.

2. SiC near-field phonon resonance

In view of the rather low power from our broadband source the s-SNOM is initially aligned with the CO_2 laser beam. The reference mirror position for positive interference of all frequencies (white light position, WLP) is approximately set with the help of a ruler (the optical path length inside the NeaSNOM is 2 x 17 cm). The power efficiency of backscattering from the tip is found to be of the order of 0.25%, which corresponds to a detector signal level of about 5% of the input signal (Fig. 2). The latter is experimentally determined by an auxiliary probe arm with a full mirror.

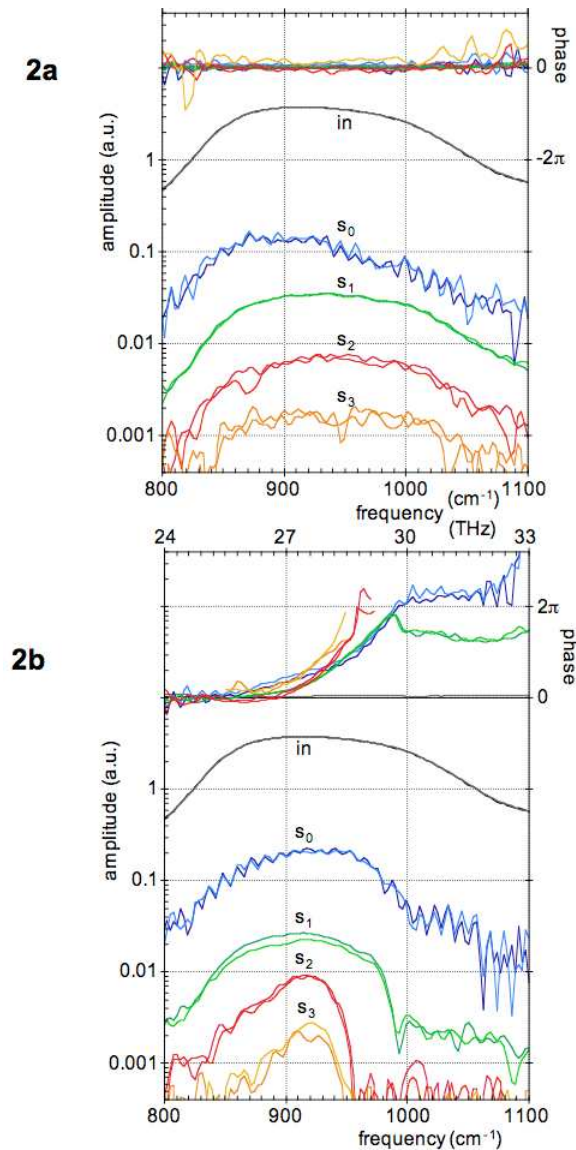


Fig. 2. Mid-infrared spectra obtained by s-SNOM of an Au sample (a) and a SiC sample (b). Amplitude spectra (lower part) are shown for the input beam (in), the directly backscattered beam (s_0), and its demodulated components at the n^{th} harmonics (s_n). The corresponding phase spectra (upper part) are shown in the same colours. The WLP was chosen such that the phase is nearly constant for the $n = 1$ phase spectrum of Au. The tapping amplitude was set to 100 nm.

Similar as in earlier reports [9,11,12], the modulated amplitudes of backscattering are found to decrease with n , here roughly by a factor 5 per harmonic order. With the non-resonant Au sample the spectral shapes are similar to that of the input spectrum, except for the direct scattered one, s_0 ; its distortion resembles that found earlier with a different tip shape, and may indicate antenna resonance [13]. The phase spectra are flat and unshifted within 20° which means the locus of backscattering remains within ± 140 nm constant for all spectral elements. Approach curves (not shown) are regularly taken, with the interferometer kept fixed, to ascertain that the $n = 2, 3$ responses are dominated by near-field interaction.

Figure 2b displays the spectra obtained with a SiC sample which possesses a well-studied near-field phonon resonance in the mid infrared [4,9,13–17]. As expected for this resonance,

the amplitude spectra for $n = 2, 3$ exhibit a ca. 60 cm^{-1} wide peak (FWHM) at ca. 920 cm^{-1} exceeding the value of Au. The $n = 0, 1$ spectra, in contrast, appear flat up to about 980 cm^{-1} where the amplitude markedly decreases. This is expected for the far-field response due to Fresnel reflection in the Reststrahlen region of SiC, as illustrated in Fig. 2 of ref [4]. The phase spectra exhibit a monotonic increase in the Reststrahlen region. This increase is enhanced in the near-field interaction. Our general conclusion is that spectroscopic s-SNOM generates meaningful amplitude and phase spectra. Specifically, the near-field interaction dominates the spectra from demodulation order $n = 2$ up, given the tip geometry and tapping parameters as used here.

3. Background-free detection at first harmonic

The results (Fig. 3) of a second measurement series with a different tip from the same batch indicate, in the $n = 1$ spectrum, the presence of substantial background scattering; this could come from a non-perfect alignment of the focus to the tip or may reflect an antenna property of the tip. We present this series because it illustrates a new way to recognize background contamination, by inspecting pulse-type interferograms obtainable only with broadband illumination. In Fig. 3b the centrally plotted interferogram of the input (black, scaled /100) lasts for a time span A. It can be understood as the autocorrelation of a ca. 3-cycle input pulse. Nearly congruent with it are interferograms of the two samples measured at $3 \mu\text{m}$ retraction from contact (dotted red and green). Since such a retraction must fully suppress the near-field interaction [1,11], the dotted spectra (Fig. 3a) designate pure background scattering. We assume such background spectra should prevail nearly unaltered also at contact. This is confirmed by comparison with the $n = 1$ interferogram of Au. It starts out congruently in shape with the input, but then continues ringing for a time span B. The difference of both interferograms, on and off contact, is approximately identical in shape with that of the $n = 2$ interferogram. The latter represents the pure near-field response, as concluded above from approach curves, and as also can be seen by comparing the $n = 2$ spectrum of Fig. 3a with Fig. 2b and previous reports [9,16].

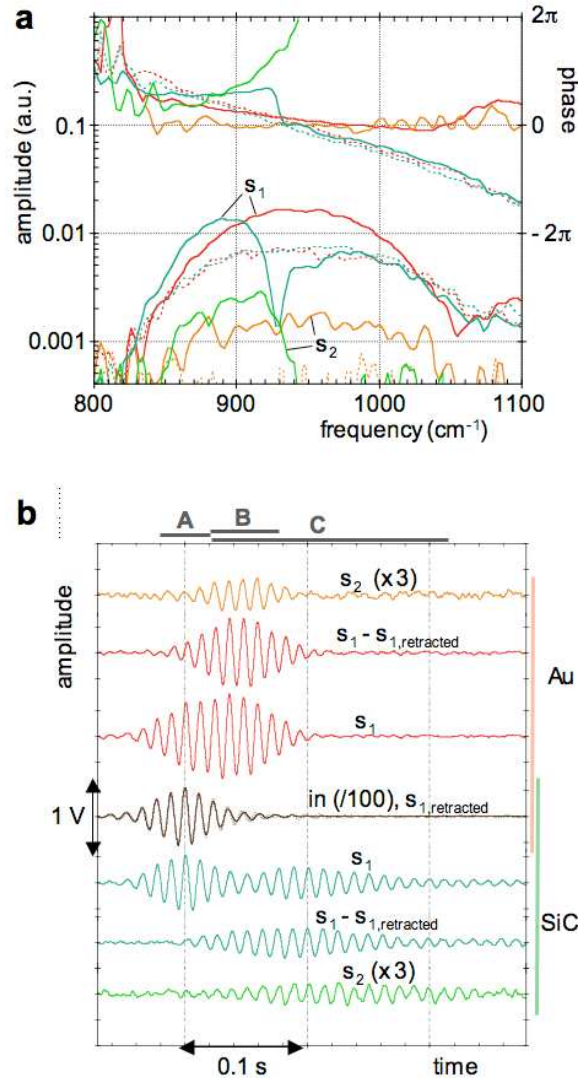


Fig. 3. Mid-infrared s-SNOM spectra (a) and corresponding interferograms (b) obtained with an Au (red, yellow) and a SiC sample (green, blue). Background scattering is present in the $n = 1$ but not in the $n = 2$ cases. The interferograms (offset for clarity) exhibit three distinguishable features, (A) background scattering signature congruent with input, (B) near-field response of Au, (C) near-field response of SiC. The tapping amplitude was set to 65 nm.

We thus suggest that the near-field response can be approximately determined even from background-contaminated $n = 1$ interferograms, during time span B, owing to the fact that the background and the near-field features appear essentially time-separated. Since the signal level for $n = 1$ is about 5x larger than for $n = 2$, the choice of using $n = 1$ interferograms instead of $n = 2$ interferograms has a decisive advantage for performing the initial s-SNOM setup because it requires a 25x shorter measuring time for the same S/N ratio. Note that, in contrast, the *spectral* curves (red, full and dotted, in Fig. 3a) would give no hint of the presence of a background. Our observation is corroborated by the interferograms taken with the SiC sample (Fig. 3b). In these, the ringing lasts for a prolonged time span C. Furthermore, it starts with a substantial phase shift compared to the background feature, which leads to a minimum in the s_1 envelope. Both features are related to the phonon resonance of SiC. The

relatively long ringing marks the high quality factor owing to substantial energy stored in the cavity formed by the tip apex and the sample.

4. Free-induction decay

A prolonged response (ringing) is well known as free-induction decay (FID) in many other fields of coherent spectroscopy mainly of quantum systems such as spin or vibrational/electronic two-level systems. What we observe here is the first evidence of FID in a classical near-field coupled system, namely a scatterer close to a material surface. While implications and analogies with quantum systems are beyond the scope of this letter, we emphasize the FID's interesting practical application for s-SNOM adjustment and operation as already explained. We add another aspect, which may be of high interest in future studies. The interferogram could detect retardation generated by internal delay within a complex scatterer caused, for example, by surface plasmon propagation as considered in refs [18,19]. Intra-scatterer retardation as small as 10° could be detected, which at $1 \mu\text{m}$ wavelength would correspond to a propagation time as short as 83 as.

5. Influence of tapping amplitude

To probe the influence of the tapping amplitude on both background and near-field signals we performed a systematic variation and display the result in Fig. 4.

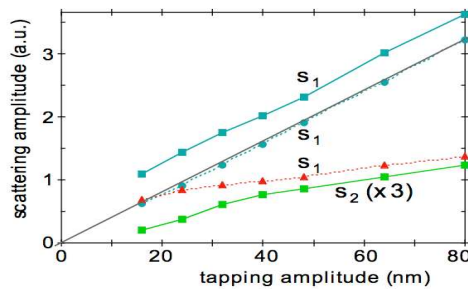


Fig. 4. Experimental, spectrally averaged s-SNOM amplitude of SiC (squares), of SiC retracted $3 \mu\text{m}$ away from contact (dots), and of the difference (triangles) vs tapping amplitude. Connecting curves and the straight line are guides to the eye only.

A linear behaviour is found for the pure background signal (dots at $n = 1$), as to be expected, whereas the other curves show a saturated behaviour obviously due to the near-field parts. In the $n = 1$ case, for example, at 20 nm the near-field part obtained by subtracting the off-contact from the on-contact interferograms (triangles) equals that of the background (dots), but at 50 nm tapping amplitude it amounts to only 50%. This trend is in accord with earlier estimations [20,21]. These predict a slowed increase of the near-field amplitude once the tapping amplitude exceeds the size of the near field, which is of the order of the tip radius, typically 20 nm in our study.

6. Proximity effect

As a final illustration of broadband s-SNOM spectra we demonstrate the influence of a nearby scattering object, the edge of an Au film, which is situated towards the focusing mirror. From former studies of plasmon-resonant scatterers [22–24] or edge scatterers [25] we expect to obtain an increased scattering caused by the additional illumination of the tip due to the proximal scatterer. The results show that such an enhancement indeed occurs, amounting to factors between 2 and 4, and that the spectral signatures stay largely unaffected (Fig. 5).

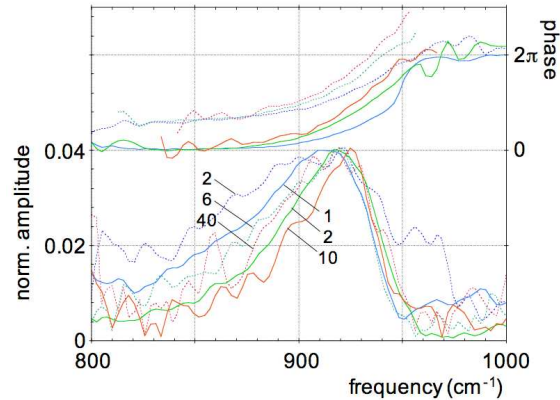


Fig. 5. Mid-infrared spectra obtained by s-SNOM on SiC, 100 μm (full) and 100 nm away (dotted) from a 25 nm high Au film, normalized to the input spectrum. Colour code as in Fig. 2: s_0 blue, s_1 green, s_2 red. The amplitudes are scaled by the factors indicated. The dotted phase spectra are offset for clarity. The tapping amplitude was set to 70 nm.

7. Conclusion

The spectra shown in this work were acquired by averaging 10 to 100 interferograms, each lasting 2 s. A boost of the present beam power of 5 μW by at least an order of magnitude would eliminate the need of averaging, and ease the way to spectroscopic near-field images. Altogether, we have shown a robust setup and procedure which uses a broadband light source for illumination and for obtaining local spectra. Our setup requires less installation cost and less computational effort than the former coherent dual frequency-comb system [9]. The present method can readily be used with other types of light sources such as synchrotrons and in other frequency ranges such as, for example, covered by a white light continuum beam.

Acknowledgements

We acknowledge discussions with M. Brehm, A. Schliesser, N. Ocelic, R. Hillenbrand, and A. Apolonskiy. Supported by Deutsche Forschungsgemeinschaft through Cluster of Excellence Munich-Centre for Advanced Photonics.